PULSED LASER INTERACTIONS WITH SILICON NANOSTRUCTURES IN EMITTER FORMATION

(Interaksi Denyutan Laser dengan Nano-Struktur Silikon dalam Pembentukan Pemancar)

Victor Lim Chee Huat*, Cheow Siu Leong, Kamaruzzaman Sopian, Saleem Hussain Zaidi

Solar Energy Research Institute (SERI),
Universiti Kebangsaan Malaysia, 43600 UKM Bangi, Selangor, Malaysia

*Corresponding author: victorlimch@yahoo.com

Abstract

Silicon wafer thinning is now approaching fundamental limits for wafer thickness owing to thermal expansion mismatch between Al and Si, reduced yields in wet-chemical processing as a result of fragility, and reduced optical absorption. An alternate manufacturing approach is needed to eliminate current manufacturing issues. In recent years, pulsed lasers have become readily available and costs have been significantly reduced. Pulsed laser interactions with silicon, in terms of micromachining, diffusions, and edge isolation, are well known, and have become industrial manufacturing tools. In this paper, pulsed laser interactions with silicon nanostructures were identified as the most desirable solution for the fundamental limitations discussed above. Silicon nanostructures have the capability for extremely high absorption that significantly reduces requirements for laser power, as well as thermal shock to the thinner wafer. Laser-assisted crystallization, in the presence of doping materials, leads to nanostructure profiles that are highly desirable for sunlight absorption. The objective of this paper is the replacement of high-temperature $POCl_3$ diffusion by laser-assisted phosphorus layers. With these improvements, complete low-temperature processing of thinner wafers was achievable with 3.7 % efficiency. Two-dimensional laser scanning was proved to be able to form uniformly annealed surfaces with higher fill factor and open-circuit voltage.

Keyword: pulsed laser interactions, silicon nanostructures, laser-assisted crystallization

Abstrak

Penipisan wafer silikon pada masa ini sudah mendekati had asas ketebalan wafer kerana ketakserasian pengembangan terma antara Al dan Si, pengurangan hasil dalam proses kimia basah adalah disebabkan oleh kerapuhan, dan pengurangan penyerapan optik. Pendekatan pembuatan adalah diperlukan supaya mengatasi masalah pembuatan semasa. Kebelakangan ini, denyutan laser sudah tersiap sedia dan kos telah ternyata berkurang. Interaksi denyutan laser dengan silikon dari segi pemesinan mikro, pembuaran, dan pengasingan tepi sudah diketahui umum dan menjadi alat pembuatan industri. Dalam makalah ini, interaksi denyutan laser dengan nano-struktur silikon telah dikenal pasti sebagai penyelesaian paling dikehendaki kepada had asas yang telah dibincangkan diatas. Nano-struktur silikon mempunyai kebolehan penyerapan yang teramat tinggi sehingga mampu mengurangkan kuasa laser diperlukan dan juga renjatan terma kepada wafer yang lebih nipis. Penghabluran bantuan laser dengan kewujudan bahan tambah telah membawa kepada pembentukan nano-struktur yang mempunyai penyerapan cahaya matahari yang lebih dikehendaki. Objektif makalah ini telah dikenal pasti sebagai pengantian pembauran $POCl_3$ suhu tinggi oleh lapisan forforus bantuan laser. Dengan kemajuan ini, pemprosesan wafer yang lebih nipis pada suhu rendah secara menyeluruh telah dicapai dengan kecekapan 3.7%. Dua dimensi imbasan laser telah dibuktikan dapat membentuk permukaan lindapan yang seragam dengan faktor isi dan voltan litar buka yang lebih tinggi.

Kata kunci: interaksi denyutan laser, nano-struktur silikon, penghabluran bantuan laser

Introduction

Crystalline Si solar cells represent the most cost-effective and environmentally friendly renewable energy generation option [1]. Their dollar/watt cost of silicon-based photovoltaic is still high in comparison with carbon-based, fossil-fuel resources. A highly effective approach for Si PV cost reduction is through the economic use of silicon in the form of thinner wafers [2]. Over the years, silicon wafer thickness has been gradually reduced; current wafer thickness is in the ~ 180–150 μm range. This evolutionary approach is now approaching fundamental limits owing to several factors, including thermal expansion mismatch between Al and Si, reduced yields in wet-chemical processing as a result of increased fragility [3], and reduced optical absorption. Therefore, alternate manufacturing approaches are required in order to continue reducing energy-conversion costs.

Laser doping research began during the 1960s, with applications for solar cells gaining prominence in the late 1970s and early 1980s, generating 'spatially localized doping patterns' in 'efficient Si solar cells by laser photochemical doping' [4]. The broader use of lasers to assist selective emitter formation was pioneered at the University of New South Wales (UNSW) during the mid-1980s [5], and through EU-funded programmes called 'Low-Therm-Cells' [6] and 'Light-Print-Cells' [7], which featured 'the use of spin-on techniques and laser-assisted treatments to get selective emitter structures'. These feature a heavily-doped contact area underneath the metallised region and a lightly doped emitter area between front fingers. But even here, different schemes are proposed, each with unique processes and equipment. Recently, several selective emitter technologies have been developed for the purpose of implementation in industrial mass production, including silicon ink techniques [8], heavily doped emitter etch-back process [9], patterned ion implantation process through a mask [10], oxide mask process using an oxide layer as the diffusion barrier [11], and phosphorous paste printing on light phosphorous doped emitter [12].

Deposition techniques such as spin-on [13] and spray are other deposition techniques used to realize the n^+ emitter on silicon wafers. The spray technique commonly used for thin films (like tin dioxide and zinc oxide) and other transparent conductive oxides is also well suited to deposit anti-reflective coating and an aluminium or boron back surface field. This technique is simple to handle and can be characterized by a high rate production compared to the above cited techniques, even the gaseous diffusion from a phosphoryl chloride (POCl$_3$) source. These specifications are of prime importance to meet global sustainable development through the emergence of a photovoltaic industry in developing countries where sophisticated and expensive equipment are seldom available.

In this paper, pulsed laser interactions with silicon nanostructures have been identified as the most desirable solution to fundamental limitations. Pulsed lasers at affordable costs have become readily available. Pulsed lasers with pulse durations in micro to femto-second range find a wide range of applications. In this proposal, the focus is on solar cell applications. In industrial solar cell manufacturing, lasers have been used for doping, edge isolation, thru-wafer etching, scribing, dicing, epitaxial recrystallization, and dielectric film etching. Laser interaction with silicon nanostructures is of critical important due to several factors such as extremely high absorption that significantly reduces thermal budget, ability to re-crystallize, and tune texture profile for enhanced absorption in thin silicon wafers.

Based on these considerations, laser-assisted doping of nanostructured silicon solar cells was proposed. Laser-doped surfaces were screen-printed low temperature Ag paste, thereby reducing conventional 1000 °C metallization process to ~ 200 °C. The advantages of the proposed solar cell manufacturing, in comparison with conventional industrial process, can eliminates high (~ 875 - 1000 °C) temperature furnace processes based on toxic POCl$_3$ gas and boron tribromide (BBr$_3$) gas sources. Both of these gases are corrosive and harmful to human body. At the same time, thermal budget of the emitter formation process was also reduced by elimination of long furnace heating. Besides that, conventional high (~ 1000 °C) temperature rapid thermal firing for metallic contacts through the heating conveyor belt can also be eliminated and replaced by low temperature Ag paste in heating oven (~ 200 °C).

Materials and Methods

For all the works in this study, an YMS-50D laser scribing machine was used. The laser optical system consists of a laser pump cavity (including an Nd:YAG rod and a laser diode) situated on a cast-iron base, laser resonator, a Q-switch and a diode laser alignment device. The laser resonator consists of a rear mirror, a front mirror, and two mirror mounts. The rear mirror coated with a multilayer dielectric film (hard coating) reflects nearly 100% of the

laser beam at 1.064 μm. The front mirror reflects a portion of the 1.064 μm laser beam (90%). The surface of it is also coated with a multilayer dielectric film (hard coating). The Q-switch is an important optic component in a laser optic system. It obstructs or passes the laser beam at a certain frequency to achieve high peak power. This laser is equipped with an alignment unit based on a He-Ne laser beam (0.632μm) that allows visual alignment prior to actual laser operation; laser specifications are summarized in Table 1. Figure 1 shows the optical schematic of the beam incident on the wafer through the quartz chamber. Optical adjustments on the focusing beam system can be used to control laser spot size.

Table 1. YMS-50D Laser Parameters

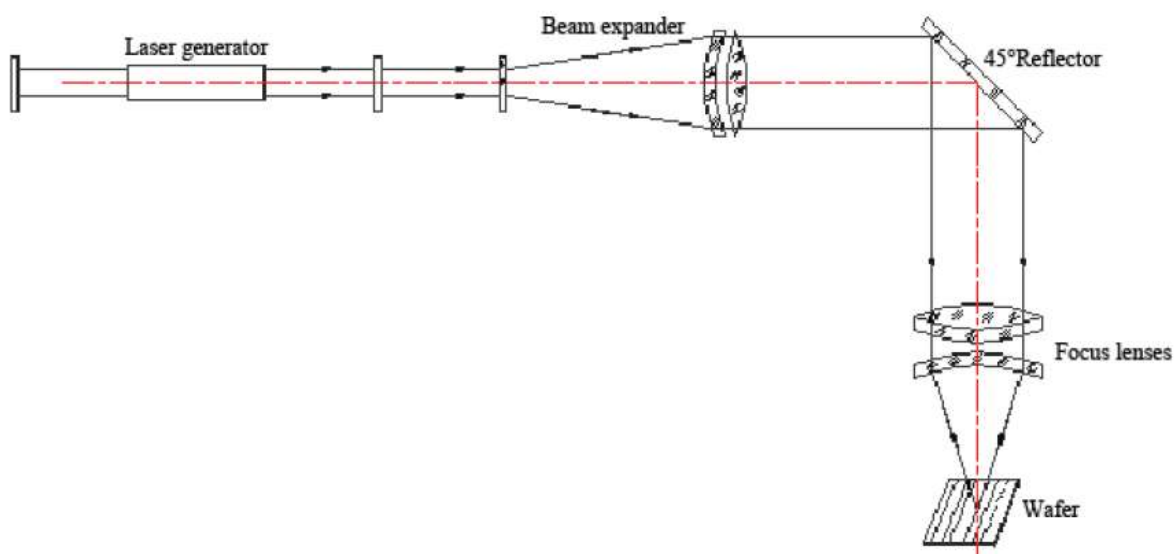| Working Material	Semiconductor Pump Laser
Wavelength	1.064 μm
Beam quality	M2＜6
Max Output Power	50W
Laser Output Instability	$\leq\pm3\%$
Modulating Frequency	0.5 kHz ~ 50 kHz
XY stage speed	0 ~ 120mm/s
Spot Size	$\leq$0.05mm
Continuous operation hours	> 24 h

Figure 1. Focusing optics for the YMS-50 D laser

The YMS-50 D laser system is equipped with a stepper-motor controller-based xy stage operating on a computer numerical control (CNC) control system that includes a motion control card controlled by computer software based on G-code. It can control translation stage at user-defined tracks and speeds. It can also control the laser generator and Q-switch to an output laser at desired positions. Figure 2 shows two examples of patterns generated by this laser by an x-y stage system. The system allows programming of any desired pattern.

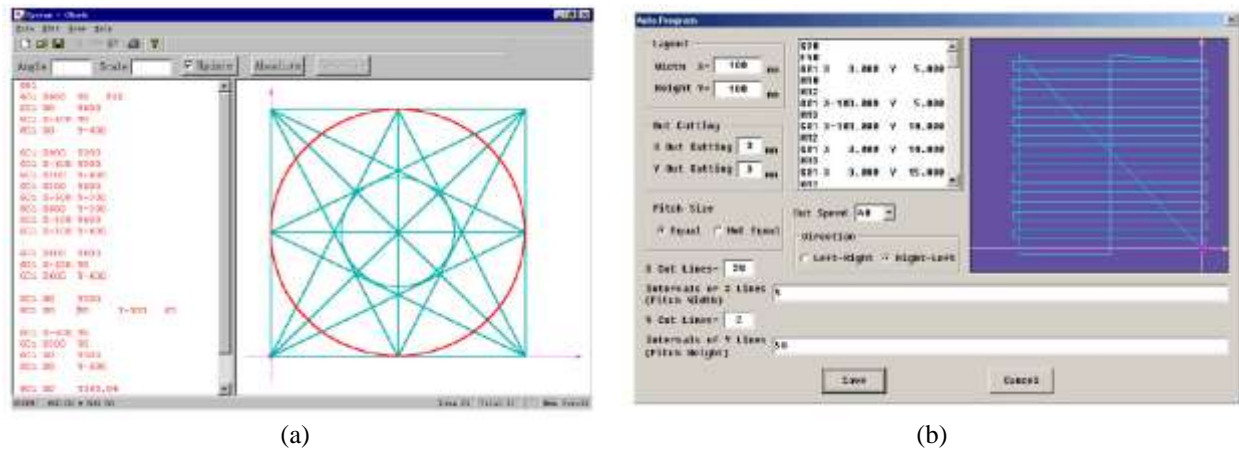(a)   (b)

Figure 2. Patterns created using YMS-50D laser system, examples of (a) circular, and (b) rectangular

Figure 3 shows the process flow for the pulsed laser interactions with silicon nanostructures in emitter formation. The process begins with saw damage removal and texturing. Silicon wafers were dipped in NaOH, H_2O: HF, IPA: KOH: H_2O and H_2O: HF solutions to remove surface damage, and create pyramid textures onto the surface of the silicon wafers. For the phosphoric acid spin-on doping step, the wafers were spray- and spin-coated with a phosphoric acid (H_3PO_4) solution. The resulting spin-on doping layers were coated as uniformly as possible across the wafer.
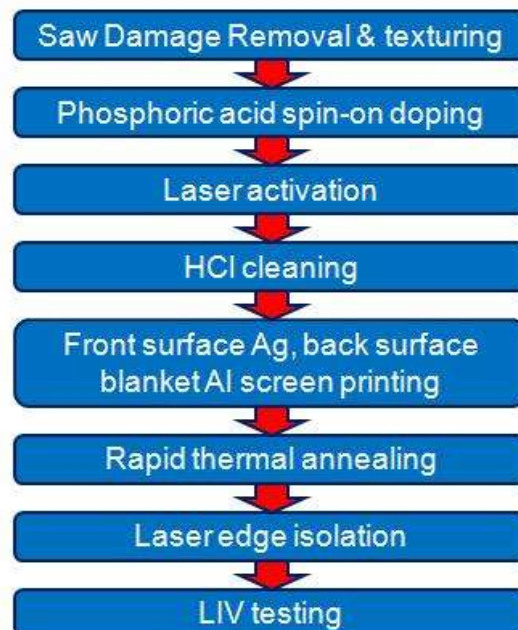

Figure 3. Pulsed laser interactions with silicon nanostructures in emitter formation process flow

A high-power laser beam was then focused onto the wafer surface with nanostructures and scanned at respective speed. During the laser irradiation time, there was sufficient heat accumulated under the focused beam to cause melting of the silicon and vaporization of the H_3PO_4 solution. Finally, diffusion of phosphorous ions into the silicon occurred, thus forming a localized, heavily-doped n^{++} emitter region. The residual of spin-on coating was rinsed using an HCl cleaning process.

After rinsing the residual spin-on dopant, the laser-doped wafers were screen-printed with low temperature curing silver paste onto the front surface, and low temperature curing aluminium onto the back surface. After that, the wafers were passed through the low-temperature rapid thermal annealing oven to create metallization. Finally, the wafer edges were sliced by a laser scribing machine to isolate short-circuit contact in between n and p regions at the edge of the wafer. After all laser interactions with silicon nanostructures in emitter formation process finished, the fabricated solar cells were characterized by an LIV tester to study the solar cells' performance. The surfaces of the wafer, which interacted with a pulsed laser, were examined using a scanning electron microscope (SEM).

Results and Discussion

Figure 4 shows the SEM pictures of the laser annealing of nanostructured Si surfaces under different magnification. Figure 4(a) shows the boundary between Si nanostructures and laser-annealed surfaces. Pulsed laser absorption in nanostructured surfaces leads to recrystallization of nanostructures into planar surfaces. The diameter of the laser beam is approximately 25 μm. Annealed regions have a width of ~ 20 μm, as shown in Figure 4(b). Annealed surfaces exhibit transverse features reflecting presence of higher order TEM modes in the beam (Figure 4(c)).
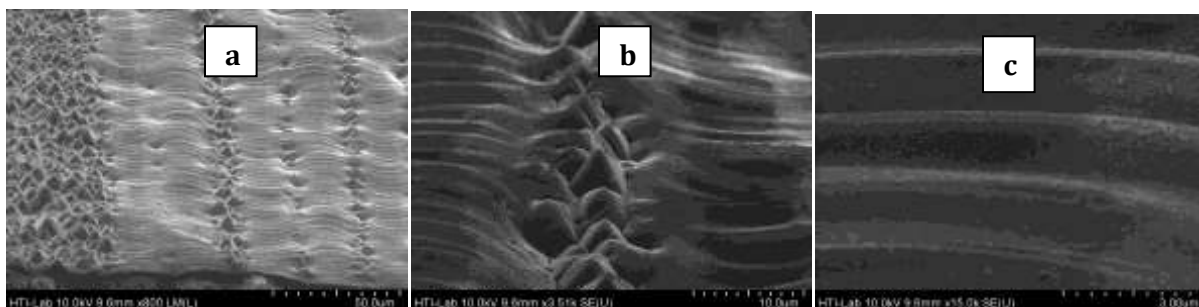

Figure 4. Laser-annealed Si surfaces under different magnification, (a) triangular-profiled Si nanostructures under magnification 800, (b) laser re-crystallization of Si nanostructures under magnification 3.5k, and (c) view of the laser-annealed surface under magnification 15k

In order to form uniformly laser-annealed surfaces, several computer programs were written, based on the simple configuration identified in Figure 2(b). Nanostructured Si samples were placed on the stage and the laser was scanned at different periods. Figure 5 shows SEM pictures of one-dimensional laser scans at 50-μm periods. SEM pictures exhibit non-uniformities likely attributed to stage translation. The laser spot size varies between 10 and 20 μm. Figure 6 shows high-resolution SEMs of the same sample showing a relatively uniform concave planar region.
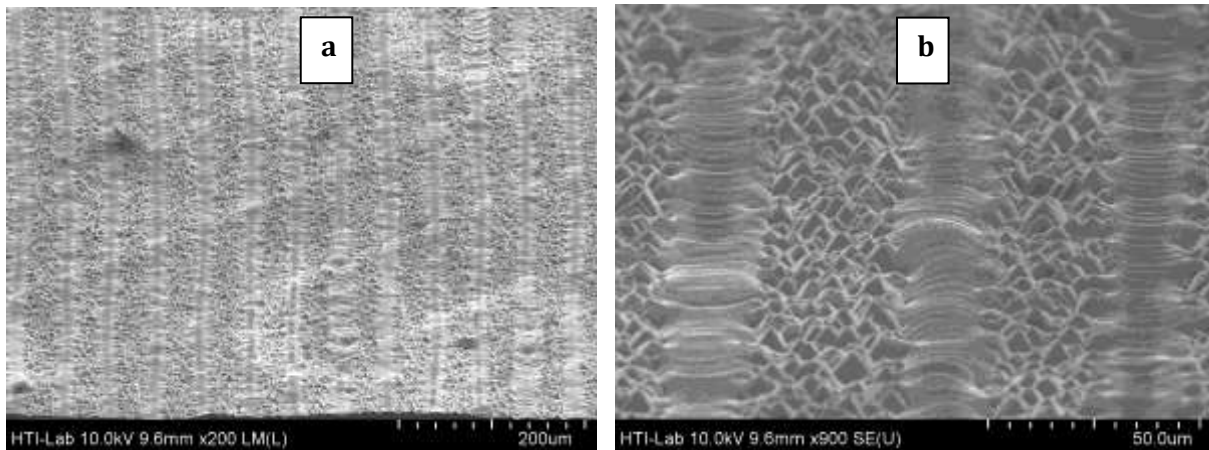
Figure 5. SEM image of one-dimensional laser-scanned annealing at 50-μm period under different magnification,(a) under magnification 200, and (b) under magnification 900
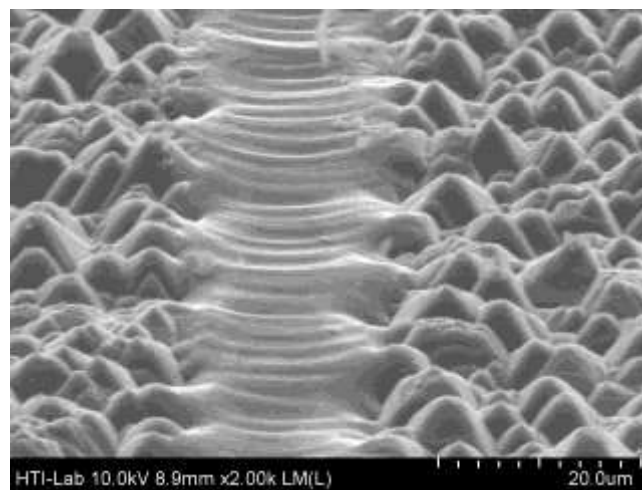

Figure 6. High resolution SEM pictures of one-dimensional laser-scanned surfaces at 50-μm period

Figures 7 and 8 show the SEM pictures of one-dimensional laser scans at 25-μm periods. SEM pictures exhibit non-uniformities likely attributed to stage translation. Figure 7 (a) also shows a contrast between the centre and the edges of laser-annealed regions, indicating energy variation across the beam profile. Figure 8 shows the unannealed region is approximately 5-μm wide.
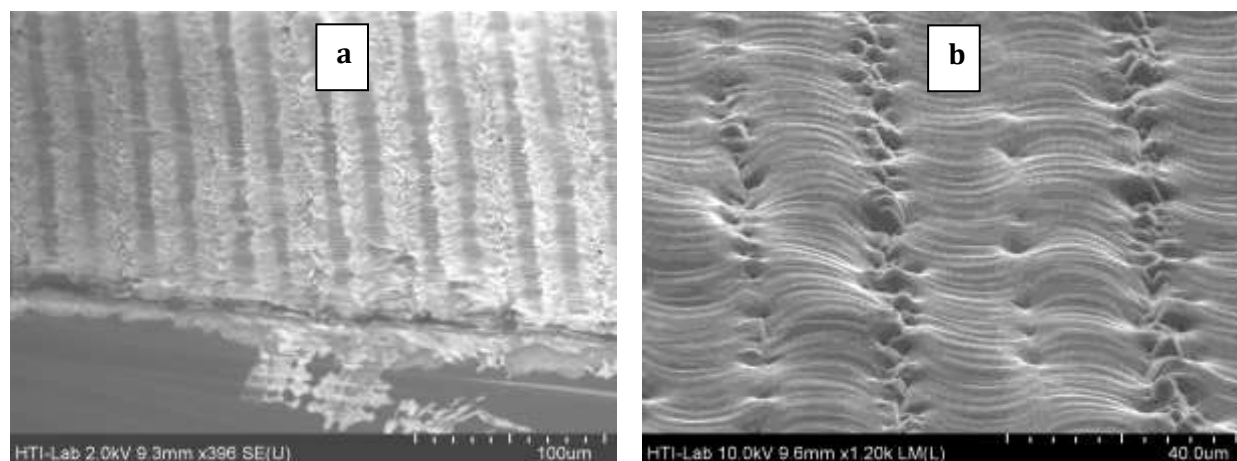
Figure 7.   SEM image of one-dimensional laser-scanned annealing at 25-μm period under different magnification, (a) under magnification 396, and (b) under magnification 1.2k
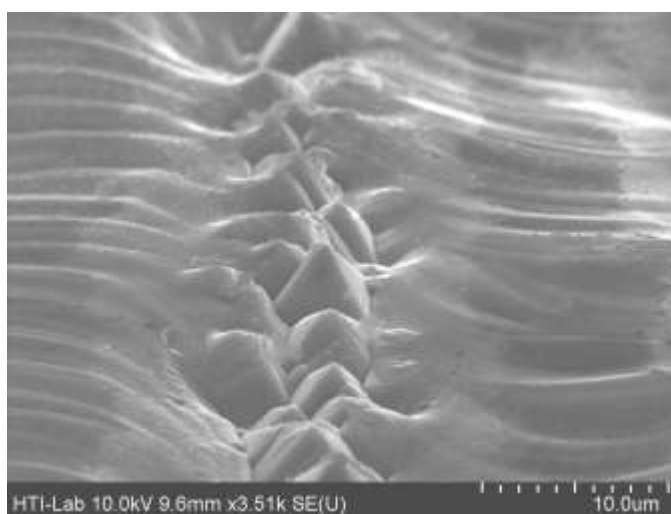

Figure 8. High resolution SEM pictures of one-dimensional laser-scanned surfaces at 25-μm period

One-dimensional laser annealing scans indicate that two-dimensional scanning may be required to form uniformly annealed surfaces. Figures 9 and 10 show SEM pictures of two-dimensional laser scans at 50 and 25-μm periods, respectively. At 50-μm, significant areas are left unannealed (Figures 9 (a)–(c)). The pyramid structures are still visible in all the figures in Figure 9. At 25-μm periods, almost the entire surface is uniformly annealed (Figures 10 (a)–(c)). These preliminary measurements indicate that for fixed laser parameters, two-dimensional laser scanning at periods slightly less than 25-μm would be required to form uniformly surfaces.
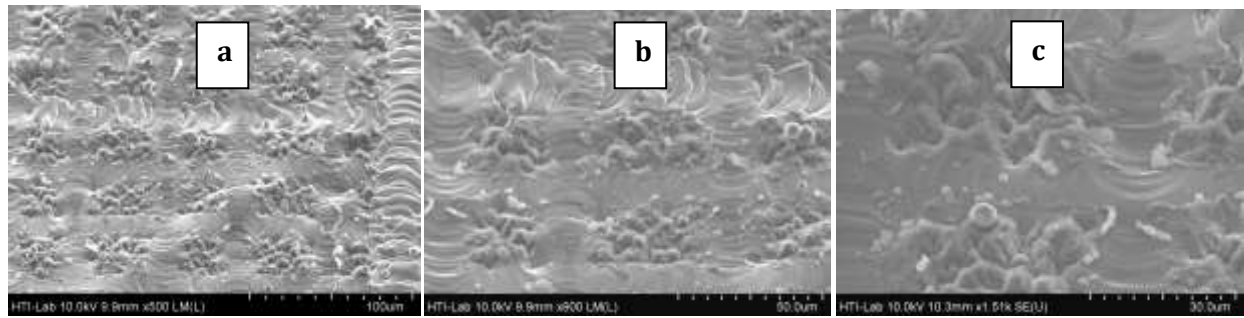
Figure 9. SEM pictures of two-dimensional laser-scanned surfaces at 50-μm period under different magnification, (a) under magnification 500, (b) under magnification 900, and (c) under magnification 1.5k
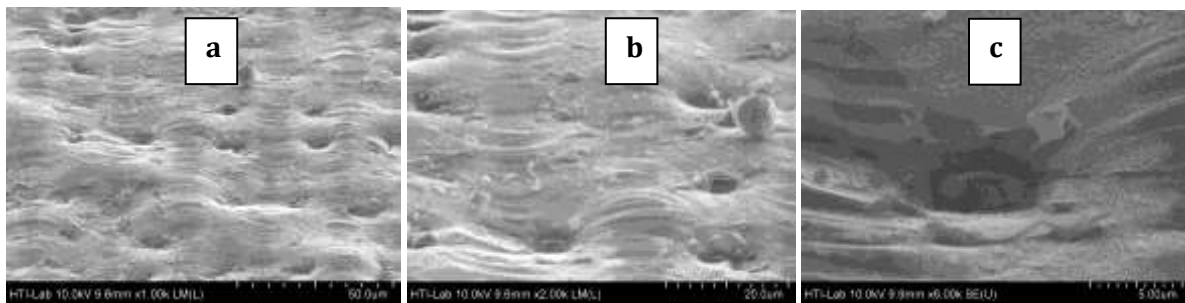

Figure 10. SEM pictures of two-dimensional laser-scanned surfaces at 25-μm period under different magnification, (a)under magnification 1k, (b) under magnification 2k,and (c) under magnification 6k

Figure 11 shows the LIV data for one-dimensional and two-dimensional laser annealing scan solar cells. The results shows that the one-dimensional laser annealing scan solar cell has a very low fill factor and open-circuit voltage (V_{OC}). This is because the laser annealing lines don't connect between one another. This creates a very high resistant region in between each of the lines. The non-annealed regions also lower the V_{OC}. The result shows that the two-dimensional laser annealing scan solar cell has a higher fill factor and V_{OC}. This is because the laser annealing lines are connected between one another. This lowers the resistant region in between each of the lines. The fully annealed regions also provide higher V_{OC}. The one-dimensional laser annealing scan solar cell has a higher short-circuit current (Jsc) because some pyramid nanostructures still remain after the one-dimensional scan. This made one-dimensional laser annealing scan solar cell absorb more light and created a higher Jsc. The experimental solar cell efficiency is 0.53 % for the one-dimensional laser annealing scan. The experimental solar cell efficiency is 3.7 % for the two-dimensional laser annealing scan.

The laser-based solar cell configurations were also investigated using PC1D simulation. The solar cell was based on the laser activation of the spin-on phosphoric acid film, with conventional back surface Al BSF contact. Figure 12 plots the experimental data along with the best fit of the data. The solar cell efficiency was calculated to be 3.7 % in PC1D simulation, which is matched by the experimental result. Good agreement is seen between experimental data and theoretical fit; process parameters used for fitting the data are listed in Figure 12.
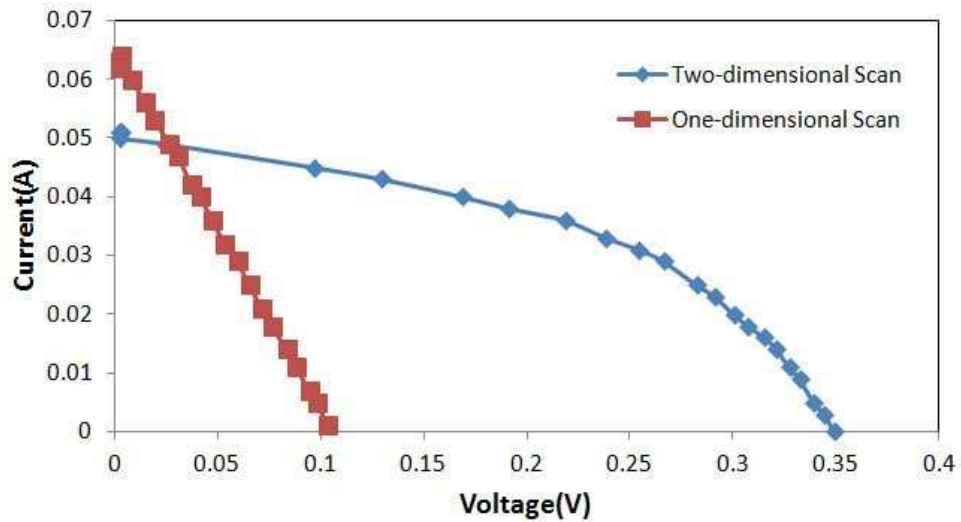
Figure 11. LIV data for one-dimensional and two-dimensional laser annealing scan solar cell
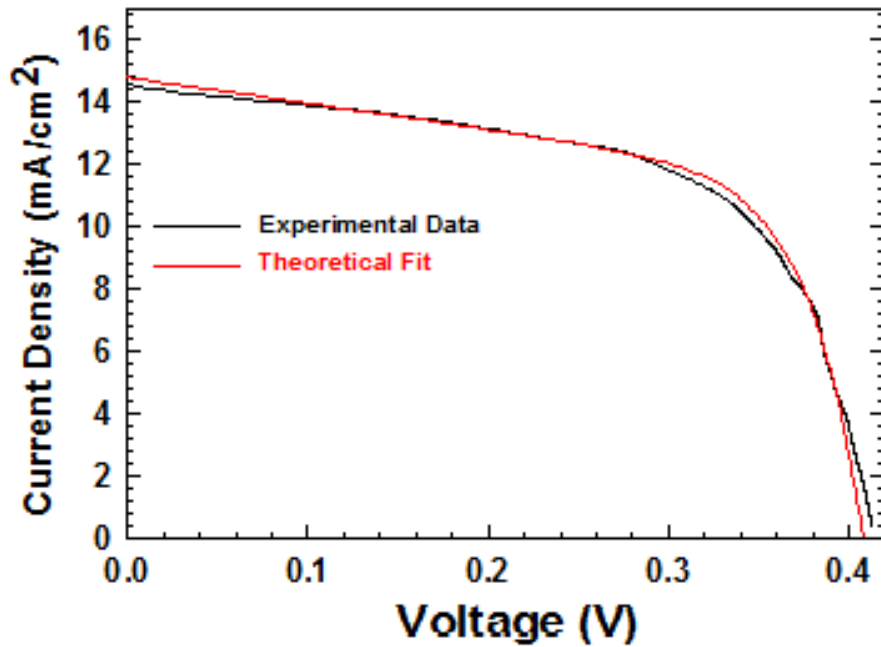

Figure 12. Comparison between experimental data and simulation data with the best fit of the data. Parameter conditions; Lifetime= 0.02 μsec, Shunt resistant= 50 Ω, Doping concentration= 2.87e16, Reflectance= 40%, Emitter resistant= 0.05 Ω

Conclusion

In summary, pulsed laser interactions with silicon nanostructures processes have been studied. Two-dimensional scanning is the better scanning technique because it is able to form uniformly annealed surfaces. Two-dimensional scanning also shows that the solar cell has a higher fill factor and open-circuit voltage (V_{OC}). A solar cell with 3.7 %

efficiency was created by two-dimensional scanning technique. PC1D simulation was carried out with the existing parameters of the solar cell and has a good agreement with experimental data. Further optimization on laser beam size might need to be carried out to increase the V_{oc}, fill factor and efficiency.

Acknowledgement

References

1. Green, M.A. (2003). Crystalline and Thin-film Silicon Solar Cells: State of The Art and Future Potential. *Solar Energy*, 74(3): 181-192.
2. Munzer, A.A., Holdermann, K.T., Schlosser, R.E. and Sterk, S. (1999). Thin Monocrystalline Silicon Solar Cells. *IEEE Transactions on Electron Devices*, 46 (10): 2055-2061.
3. Funke, C., Sciurova, O., Möller, H. J., Stephan, M., Fröhlich, K. J., Seifert, C., Bachmann, A. and Müller, A. (2004). Towards thinner wafers by multi-wire sawing. *Proc. 19th European Photovoltaic Solar Energy Conference*: 1266.
4. Deutsch, T. F., Fan, J. C. C., Turner, G. W., Chapman, R. L., Ehrlich, D. J. and Osgood, R. M. (1981). Efficient Si Solar Cells by Laser Photochemical Doping. *Applied Physics Letters*, 38(3): 144-146.
5. Green, M.A. (1995). *Silicon solar cells: Advanced principles and practice*. Sydney: Center for Photovoltaic Devices.
6. Besu-Vetrella, U., Pirozzi, L., Salza, E., Ginocchietti, G., Ferrazza, F., Ventura, L., Slaoui, A. and Muller, J.C. (1997). Large Area, Screen Printed Silicon Solar Cells with Selective Emitter Made by Laser Overdoping and RTA Spin-on Glasses. *IEEE 26th Photovoltaic Specialists Conference*: 135-138.
7. Pirozzi, L., Arabito, G., Artuso, F., Barbarossa, V., Besi-Vetrella, U., Loreti, S., Mangiapane, P. and Salza, E. (2001). Selective Emitters in Buried Contact Silicon Solar Cells: Some Low-cost Solutions. *Solar Energy Materials & Solar Cells*, 65: 287-295.
8. Antoniadis, H., Jiang, F., Shan, W. and Liu, Y. (2010). All Screen Printed Mass Produced Silicon Ink Selective Emitter Solar Cells. *Proceedings of the 35th IEEE Photovoltaic Specialists Conference*: 1193-1196.
9. Book, F., Braun, S., Herguth, A., Dastgheib-Shirazi, A., Raabe, B. and Hahn, G. (2010). The Etch Back Selective Emitter Technology and Its Application to Multi Crystalline Silicon. *Proceedings of the 35thIEEE Photovoltaic Specialists Conference*: 1309-1314.
10. Gupta, A., Low, R.J., Bateman, N.P.T., Ramappa, D., Gossman, H.J.L., Zhai, Q., Sullivan, P., Skinner, W., Dube, C., Tsefrekas, B. and Mullin, J. (2010). High Efficiency Emitter Cells using In-situ Patterned Ion Implantation. *Proceedings of the 25th European Photovoltaic Solar Energy Conference*: 1158-1162.
11. Ester-Breton, A., Beanie, F., Breselge, M., Friess, T., Geiger, M., Holbig, E., Isenberg, J., Keller, S., K¨uhn, T., Maier, J., M¨unzer, A., Schlosser, R., Schmid, A., Voyer, C., Winter, P., Bayer, K., Kr¨umberg, J., Henze, S., Melnyk, I., Schmidt, M., Klingbeil, S., Walter, F., Kopecek, R. and Peter, K. (2009).Crystalline Silicon Solar Cellswith Selective Emitter for Industrial Mass Production. *Proceedings of the 24th European Photovoltaic Solar Energy Conference*: 1068-1071.
12. Jourdan, J., Popescu, L. M., Halm, A. and Kopecek, R. (2009). Selective Emitter Solar Cellson P-type Solar Grade Silicon Wafers. *Proceedings of the 24th European Photovoltaic Solar Energy Conference*: 1784-1787.
13. Shimokawa, R., Nishida, K., Suzuki, A. and Hayashi, Y. (1987). Solar Cell Characteristics of High-Efficiency Polycrystalline Silicon Solar Cells Using SOG-Cast Wafers. *Japanese Journal of Applied Physics*, 26(10): 1667-1673.